Available online at www.sciencedirect.com
ScienceDirect
Journal of Power Sources 170 (2007) 450–455
JOURNAL OF POWER SOURCES
www.elsevier.com/locate/jpowsour

Short communication

Fabrication and properties of macroporous tin–cobalt alloy film electrodes for lithium-ion batteries

Fu-Sheng Ke, Ling Huang *, Hong-Bing Wei, Jin-Shu Cai, Xiao-Yong Fan, Fang-Zu Yang, Shi-Gang Sun *

Department of Chemistry, College of Chemistry and Chemical Engineering, State Key Laboratory of Physical Chemistry of Solid Surfaces, Xiamen University, Xiamen 361005, China

Received 28 September 2006; received in revised form 28 March 2007; accepted 4 April 2007
Available online 18 April 2007

Abstract

The Sn-based intermetallic compounds possess a high specific energy density, but their most important challenge to be used as anodes in lithium ion batteries consists in the mechanical fatigue caused by volume change during lithium intercalation and extraction processes. The current paper presents a facile procedure to prepare macroporous Sn–Co alloy film electrode through a colloidal crystal template method together with electroplating on a Ni-coated Cu sheet substrate. The structure and electrochemical properties of the macroporous Sn–Co alloy films were examined by scanning electron microscopy (SEM), X-ray diffraction (XRD), X-ray photoelectron spectroscopy (XPS), and galvanostatic cycling. The results illustrated that the macroporous Sn–Co alloy film electrode can deliver a reversible capacity as high as 610 mAh g^{-1} up to 75th cycle. In comparison with the Sn–Co alloy film directly deposited on Ni-coated Cu sheet substrate, the macroporous structure of the Sn–Co alloy electrode prepared by the present procedure has enhanced significantly the capacity and the cyclic performance. It has demonstrated that the macroporous structure has played an important role, in addition to the alloying effect, to overcome the effect of volume expansion during charge/discharge cycling of Sn-based alloy anodes.
© 2007 Elsevier B.V. All rights reserved.

Keywords: Macroporous Sn–Co alloy; Electroplating; Colloidal crystal template; Lithium ion batteries

1. Introduction

Due to the increase demanding, in recent year, on rechargeable batteries of higher specific energy density, the tin-based materials were attracted extensive attentions for using them as anode in lithium ion battery. In comparison with the specific capacity (372 mAh g^{-1}) of graphite materials that are commonly served as anode in commercial lithium ion battery, the specific capacity (991 mAh g^{-1}) of tin anode is much higher. However, one of the most important problems preventing tin materials to be used as anode in commercial lithium ion battery (LIB) consists in their poor cyclability owing to their significant volume changes during lithium intercalation and deintercalation, which results in cracking and crumbling of the electrode and leads to the loss of electrical contact between active materials and the current collector. Such volume effect consequently declines the reversible capacity during charge/discharge cycling [1–4]. To overcome this problem, two strategies have been adopted. One is to use intermetallic compounds or active/inactive composite alloy materials, such as Sn–Ni [5], Sn–Cu [6], Sn–Sb [1,7–9], Sn–Co [10–12], etc. These materials exhibit longer cyclability than that of pure active materials. The inactive element can buffer the large volume change and as a barrier against the aggregation of active material into large grains during Li-ion insertion and extraction processes. However, long-term cycling will result in rapid loss of the reversible capacity and rechargeability. Moreover, the introduction of the inactive material decreases the electrode energy density. The other way is to use superfine materials, such as nano-SnO_2 [13], nano-SnSb [7], and nano-Cu_6Sn_5 [14], etc. These materials show better cyclability compared with bulk materials, because of their large surface area and short ion diffusion length. However, superfine materials always aggregate severely and merge into large particles during lithium insertion

* Corresponding authors. Tel.: +86 592 2181436; fax: +86 592 2181436.
E-mail addresses: huangl@xmu.edu.cn (L. Huang), sgsun@xmu.edu.cn (S.-G. Sun).

0378-7753/$ – see front matter © 2007 Elsevier B.V. All rights reserved.
doi:10.1016/j.jpowsour.2007.04.019

and extraction [8]. The aggregation leads to significant volume change in the electrode and a gradual decline of the electrochemical capacity [9].

Recently, porous materials were received considerable attentions as promising new anode materials [15–23]. The advantages of porous electrodes consist of four aspects: (i) the large open pores allow the easy transportation of liquid electrolyte; (ii) a large number of active sites is beneficial for charge-transfer reactions because of the big surface area of the porous material; (iii) the continuous network is expected to improve electrical conductivity; (iv) numerous pores can buffer the large volume change caused by disintegration of the structure [16]. Porous materials can be deposited on substrate through various methods [24], such as infiltration, electrodeposition, ionic spraying, and laser spraying, etc. In comparison, electrodeposition presents significant advantages, particular for the deposition of thin films of macroporous materials. The microstructure of the deposits can also be easily altered by controlling the electrodeposition conditions, i.e., the chemical composition of the plating bath (e.g. by adding leveling and complexing agents), the temperature, the stirring conditions and the plating current density.

In this paper we report the fabrication of macroporous Sn–Co alloy films and their structural and electrochemical characterizations. It has demonstrated that the macroporous structure of the Sn–Co alloy films can improve effectively the cycling performance when they are used as negative electrode in the LIB.

2. Experimental

2.1. Preparation of monodisperse polystyrene spheres

Polystyrene (PS) spheres of 180 nm in diameter were synthesized by using an emulsion polymerization followed by a seed growth polymerization technique according to literature [23,25,26]. Typically, at room temperature and under stirring, distilled styrene (46 mL) and distilled crylic acid (4 mL) were added into 100 mL of deionized water purged with nitrogen before the reaction. After potassium persulphate (0.3 g) and sodium dodecylsulfate (0.2 g) were added, the temperature was gradually increased to 75 °C, and the mixture was stirred for 6 h at 75 °C. These small latex particles were used to act as seeds for further growth under the same reactive conditions. The resulting PS spheres were cleaned by centrifugation and washed three times with anhydrous ethanol, and then redispersed in anhydrous ethanol for subsequent uses.

2.2. Synthesis of self-assembled colloidal template

Colloidal crystal templates of PS spheres were prepared according to the method reported in Ref. [27] with a modification [23]. Working electrodes were prepared by electrodeposition of a nickel layer (∼1 μm) onto a copper sheet of ca. 100 μm in thickness. The arithmetic mean roughness R_a of the Ni-coated Cu sheet measured by laser microscopy (OLS1200, Olympus Optical Co., Ltd.) was 0.0 μm. It is worthwhile to note that, the PS sphere latex is acidity and corrosive. When it is dropped in the air onto the Cu sheet will be severely corroded. So the deposition of a Ni layer is important, which plays a role of anti-corrosion. The working electrode was swabbed by acetone, sonicated in propanol for 15 min, and then put it into a Teflon cell. The PS spheres solution was diluted to about 0.5 wt% by using absolute ethanol, and a volume of 0.4 cm^3 was spread over the area of the working electrode enclosed by Teflon. The sedimentation and attraction capillary force were used to pack the PS spheres. Keeping the Teflon cell in a well-closed chamber and allowing the PS spheres to deposit about 2 days have achieved the sedimentation of the PS spheres. As soon as the PS spheres settled onto the substrate, a clear ethanol layer was observed on the top of the deposit. This ethanol layer was then evaporated about one day to enable the attractive capillary force to pack the PS spheres within the template. The working electrode was taken out from the Teflon cell when all the ethanol had been evaporated. The template free substrate area was covered by epoxy resins to prevent any electrodeposition onto it.

2.3. Eletrodeposition of the macroporous Sn–Co alloy films

Electrodeposition of Sn–Co alloy film onto the PS template substrate was carried out on an electrochemistry working station CHI660A (Chenhua Co., Shanghai). The plating bath for electrodeposition of Sn–Co alloy contained 75 g L^{-1} $Na_2SnO_3{\cdot}3H_2O$, 2.5 g L^{-1} $CoCl_2{\cdot}6H_2O$, 150 g L^{-1} $C_4H_4O_6KNa{\cdot}4H_2O$, and 20 g L^{-1} $K_3C_6H_5O_7{\cdot}H_2O$. All these reagents are analytical reagents, and were purchased from Sinapharm Chemical Reagent Co., Ltd. The bath temperature was kept at 55 °C and the pH was adjusted to 7.5. The diameter of the working electrode is 1 cm. Opposed to the working electrode, a coil a large platinum wire was used served as the counter electrode. A constant current density of 0.5 A dm^{-2} was flowed allowed during the deposition for 5 min. After electrodeposition, the working electrodes were immersed in terahydrofuran (THF) bath for 2 days to dissolve away the PS template. Finally, the working electrodes were transferred to an anhydrous ethanol bath and sonication for 1 min, and then dried at 120 °C at and 10^{-3} Torr for 12 h. It has measured that the mass of the macroporous Sn–Co alloy deposited is about 0.5 mg with a thickness of about 1 μm. The macroporous Sn–Co alloy working electrode keeps the geometric surface area of the substrate, i.e. 0.785 cm^2.

2.4. Charaterization of the macroporous Sn–Co alloy films

The samples were characterized by field emission scanning electron microscopy (FE-SEM, LEO-1530 SEM system), Energy dispersive X-ray (EDX) spectroscopy, X-ray diffraction (XRD, Philips X'Pert Pro Super X-ray diffractometer, Cu Kα radiation, at 2° min^{-1} scan rate) and X-ray photoelectron spectroscopy (PHI Quantum 2000 Scanning ESCA Microprobe).

Electrochemical charge–discharge behaviors were directly investigated by assembling the macroporous Sn–Co alloy work-

ing electrode into coin cells (type CR2025) in an argon-filled glove box. The macroporous Sn–Co alloy film cathode was separated from the lithium anode by a separator material (Celgard 2400). The electrolyte is consisted of a solution of 1 M $LiPF_6$ in a mixture of ethylene carbonate (EC)/dimethyl carbonate (DMC)/diethyl carbonate (DEC) 1:1:1 (vol%) obtained from Zhangjiagang Guotai-huarong New Chemical Materials Co., Ltd. The cells were galvanostatically charged and discharged in a battery test system (NEWARE BTS-610, Neware Technology Co., Ltd., China) with a constant current density of 250 mA g^{-1} at a cut-off voltage of 0.05–2.0 V (*versus* Li/Li^+) at room temperature. Cycled electrode that was used for SEM imaging was washed three times in DMC to remove electrolyte and to avoid $LiPF_6$ deposition.

3. Results and discussion

3.1. Structural characterization of the macroporous Sn–Co alloy films

Fig. 1 shows SEM image of the template of PS spheres as previously described in Ref. [23]. It can be observed that the PS spheres are well packed together. The average diameter of the sphere is measured about 180 nm that is in consistent with the value measured from TEM result (not shown). The PS spheres were accumulated into well-ordered areas by lateral capillary forces [28] when the ethanol film becomes as thin as the particle diameter. The lateral capillary forces acts solely on particles protruding out of the ethanol surface. Due to meniscus forming between two particles, the strong capillary forces arise. Their lateral projection drags the particles together. Using ethanol as disperse media can accelerate PS spheres sedimentation. Although self-sedimentation on relatively rough substrate may contain some defects, a "faultless" colloidal crystal template is not necessary in the preparation of macroporous electrodes for the LIBs.

The electrochemical deposition of Sn–Co was carried out on the prepared template. In order to ensure the solution adequately infiltrating into voids of the template, the PS sphere template film

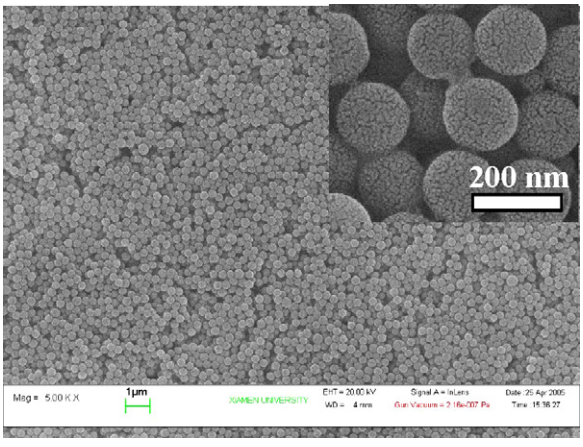

Fig. 1. SEM image of the template of PS spheres deposited on a Ni-coated Cu foil. The inset shows a corresponding high-magnification image.

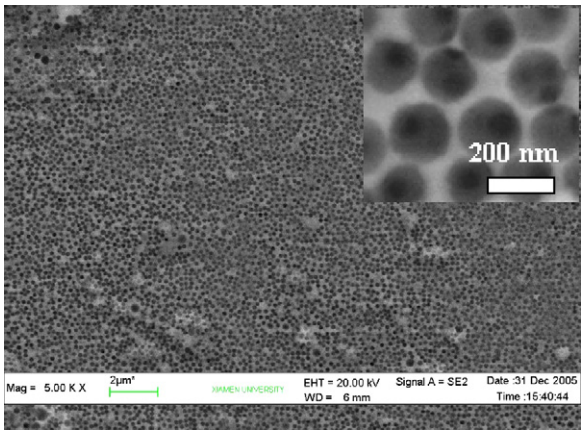

Fig. 2. SEM image of the macroporous Sn–Co alloy film after removing PS template. The inset shows a corresponding high-magnification image.

was kept in plating solution at least 15 min before electrodeposition. After passing a current, the Sn–Co alloy nuclei can nucleate on electrode surface unoccupied by PS spheres, and grow three-dimensionally. The Sn–Co alloy grew layer by layer from the substrate and filled the voids between the close-packed PS latex spheres. Some air bubbles may arise from the working electrode in process of electrodeposition if the current density is too big. Therefore, a constant current of 0.50 A dm^{-2} was applied during the deposition, which prevents the fragile templates from breaking. After the deposition of Sn–Co alloy, the PS spheres were dissolved and removed by dipping in THF for 48 h.

SEM image of the macroporous Sn–Co alloy film after removing PS template is shown in Fig. 2. We can observe holes distributed on the Sn–Co alloy layer, which interconnect to form relatively uniform pores. Such holes appear because the impregnating solid material cannot grow at the contact area of a neighboring pair of colloidal spheres in PS template. The size of pore is about 180 nm on the average. It is evident that the pores match the size of the starting PS spheres, thus indicating that the shrinkage of alloy structure can be negligible [29,30]. The continuous framework would yield advanced electronic and ionic conductivity. The thickness of the macroporous Sn–Co alloy film prepared by electrodeposition may be varied from tens of nanometer to several micrometers through varying the deposition time. However, the deposition time could not be overlong, otherwise, the upper layer of PS spheres will be wrapped and created difficulty in removing the PS sphere template by wet etching. With regard to the deposition mechanism, Bartlett et al. [31] inferred that the electrochemical deposition was initiated at electrode surface and grew out through the overlying template.

To confirm the chemical composition of the macroporous Sn–Co alloy film, it was determined by energy dispersive X-ray (EDX) spectroscopy. The EDX analysis (not show) shows that the average Sn:Co weight ratio is about 80:20 for this alloy. The crystal structure of the macroporous Sn–Co alloy films was analyzed by powder X-ray diffraction (Fig. 3). Since electroplating bath contains complex agents ($K_3C_6H_5O_7{\cdot}H_2O$ and $C_4H_4O_6KNa{\cdot}4H_2O$), the as-plated material is Sn–Co alloy

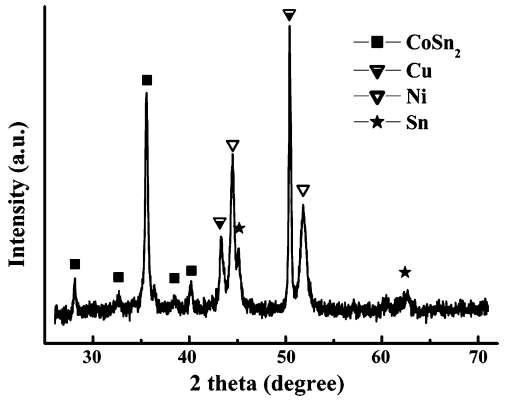

Fig. 3. XRD patterns for the macroporous Sn–Co alloy film.

rather than composite compound. The XRD result of the alloy electrode indicates the presence of two different active material phase, i.e. the main electrodeposited product of $CoSn_2$ (JCPDS no. 03-065-2697) of tetragonal structure (space group, *I*4/*mcm*), as proved by the main peaks of 2θ at 28.11°, 35.53°, and 40.16°; and a minor quantity of Sn (JCPDS no. 001-0926) of tetragonal structure (space group, *I*41/*amd*). The Sn–Co alloy is presented as a tetragonal solid solution, metallic tin as solvent and cobalt as solute. The cobalt atoms replace the tin atoms partly in the Sn–Co alloy.

The surface chemical composition of the macroporous Sn–Co alloy was also confirmed by XPS measurements. From the XPS spectra displayed in Fig. 4, we obtained the XPS survey spectrum of Co (Fig. 4a), and Sn (Fig. 4b). The Co 2p exhibits a doublet (i.e., $2p_{3/2}$ and $2p_{1/2}$) with a spin-orbit splitting of about 15.0 eV, in agreement with the literature [32]. The Co $2p_{1/2}$ and Co $2p_{3/2}$ spectra can be respectively deconvoluted into four peaks at 793.25 and 795.85 eV for Co $2p_{1/2}$, 778.20 and 779.90 eV for Co $2p_{3/2}$. The signals at 795.85 and 779.90 eV are attributed to cobalt oxide, the peaks at 793.25 and 778.20 eV to metallic Co (XPS value of pure Co $2p_{3/2}$ = 778.3 eV) [32]. The Sn 3d region exhibits a well-defined doublet with a spin-orbit splitting of about 8.32 eV [33]. It can be deconvoluted into four peaks at 493.77 and 493.33 eV for Sn $3d_{3/2}$ [34], 485.91 and 485.01 eV for Sn $3d_{5/2}$. The signals at 493.77 and 485.91 eV are assigned to tin oxide. The peak at 493.33 eV for Sn $3d_{3/2}$ is attributed to pure tin [34]. The binding of 485.01 eV for Sn $3d_{5/2}$ is close to the literature value of pure Sn (485.0 eV) [33]. Chemical analysis of the particle surface finally illustrates that the atomic ratio of Sn:Co is 48.8:51.2. This result indicates the surface of the composite contains more Co atoms than that in the inside. It may be ascribed to that more Sn ions were reduced at beginning than Co ions in the plating solution.

3.2. Electrochemical performance of the macroporous Sn–Co alloy film electrodes

The electrochemical properties of the electrode of macroporous Sn–Co alloy films are demonstrated in Fig. 5. The 1st, 2nd, 20th, 40th and 75th charge–discharge curves are show in Fig. 5a. The insertion into and the desertion of lithium ions from the macroporous Sn–Co alloy film are defined as charge and discharge of the anode, respectively. In the Li intercalation process, there was a long plateau at around 0.38 V (*versus* Li/Li^+), and then the voltage decreased gradually by 0.05 V. This is ascribed to the formation reaction of Li_xSn (x = 1–3.5) [35].

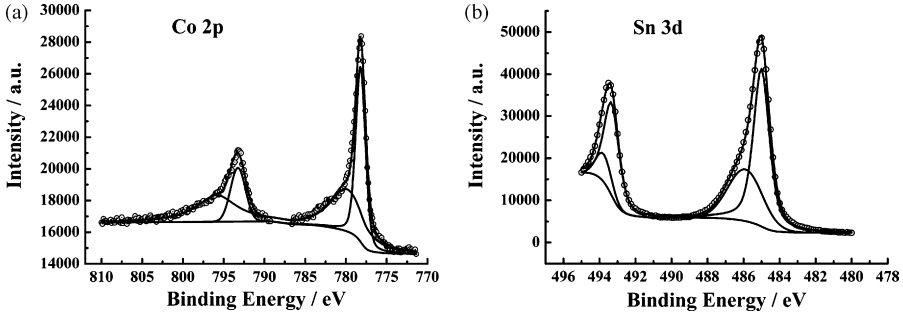

Fig. 4. XP detailed (a) Co 2p and (b) Sn 3d spectra of the macroporous Sn–Co alloy film.

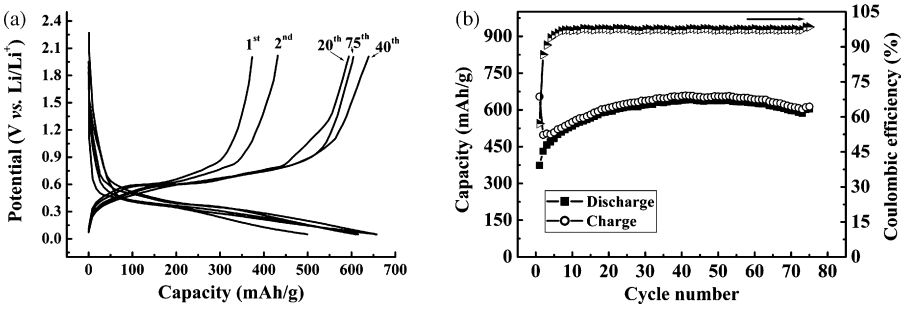

Fig. 5. (a) Charge–discharge curves of the macroporous Sn–Co alloy films. (b) Capacity and columbic efficiency *vs.* cycle number of the macroporous Sn–Co alloy films.

Fig. 5b shows the cycling behaviors of the macroporous Sn–Co alloy film electrodes. We can observe the increase in capacity in the first several cycles. It may be attributed to that the electrolyte diffuses into the internal macroporous electrode with cycles. At the first cycle, the charge capacity (intercalation) and the discharge capacity are 654.2 and 373.6 mAh g^{-1}, respectively. This indicates that the electrode exhibits a large irreversible capacity in initial charge–discharge cycle. The loss of irreversible capacity may be ascribed to (i) the formation of lithium oxides (Li_2O) from a small quality SnO_x on surface of the alloy; (ii) the formation of a solid electrolyte interphase layer (SEI) on surface with large specific surface area (due to the macroporous structure); (iii) the decomposition of electrolyte in electrode/electrolyte interphase; (iv) some lithium trapped at structural or electronic defect sites [36]. The columbic efficiencies keep as high as 97% except for the initial several cycles. At the 75th cycle, the charge capacity still remains over 93.7% of that of the first cycle. As shown in Fig. 5b, the cycling performance of the macroporous Sn–Co alloy film is exceptional. Its reversible capacity can be maintained over 600 mAh g^{-1} after 75 cycles. In comparison with the cycling performance of a $CoSn_2$ electrode reported in Ref. [12], the macroporous Sn–Co alloy exhibits excellent performance, which should be certainly attributed to the macroporous structure. The coating of a Ni layer on Cu sheet substrate does not affect the property of the macroporous Sn–Co alloy deposited on it, as evidenced by Fig. 6 in which the capacity and cycling performance of the macroporous structure electrode are significantly improved in comparison with those of a Sn–Co alloy layer directly deposited on the Ni-coated Cu sheet substrate.

SEM images of macroporous Sn–Co alloy films at different charging degree of charging are shown in Fig. 7. At 1.0 V the

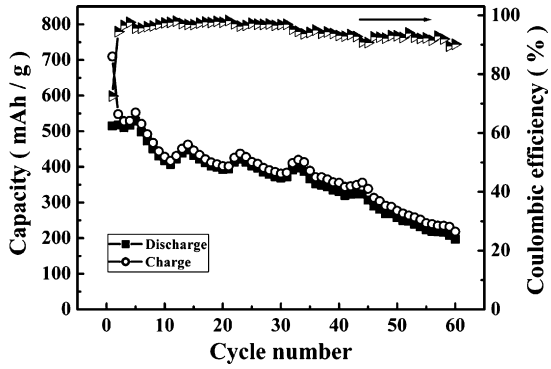

Fig. 6. Capacity and columbic efficiency *vs.* cycle number of the Sn–Co alloy electrodeposited on Ni-coated Cu sheet.

macroporous structure is similar to the original uncycled material, while the pores diameter is slightly diminished a little. The macropore size is decreased markedly at 0.4 V, indicating to the expansion of material during charging. When charging to 0.02 V, the macroporous structure is almost disappeared. After one complete cycle of charge–discharge, however, the macroporous structure is appeared again. It is worthwhile to note that the macroporous electrode may suffer also exists some aggregation during the charge–discharge cycles. However, to a large extent, the macroporous structure do have can partly accommodated the volume expansion, thus prolonged the cyclability. In addition to the accommodation of the volume expansion during charge–discharge cycles, the macroporous structure is beneficial for the diffusion of Li insertion/extraction. Such properties can improve significantly the chargeability/dischargeability at large current densities.

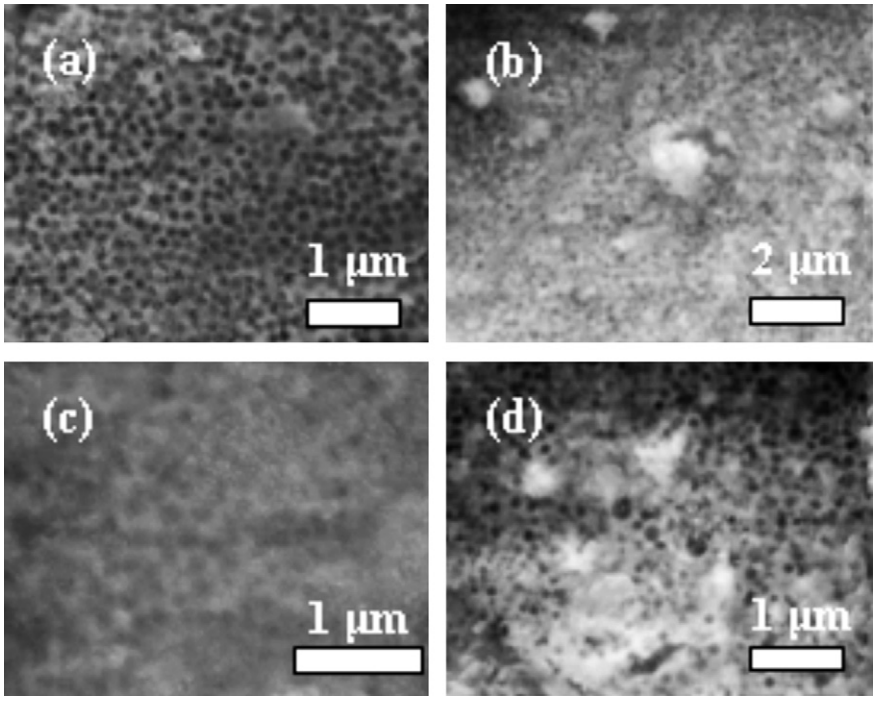

Fig. 7. SEM images acquired at different degree of charging of the macroporous Sn–Co alloy films: (a) 1 V, (b) 0.4 V, (c) 0.02 V and (d) after one complete cycle.

4. Conclusions

This paper reports the fabrication and electrochemical properties of a Sn–Co alloy anode material with a macroporous structure for lithium ion battery. The macroporous Sn–Co alloy films were prepared by electrodeposition into the interstitial spaces of a template formed by polystyrene latex spheres self-sedimentation on a relatively rough Ni-coated Cu sheet substrate. The capacity and cycling performance of the macroporous Sn–Co alloy film served as anode of lithium-ion battery were significantly enhanced in comparison with those of directly electrodeposited Sn–Co alloy on Ni-coated Cu sheet. It has revealed that the good capacity retention and cyclability are associated to the macroporous structure. The Sn–Co alloy film with macroporous structure exhibited good cycling stability, by which 93.7% reversible capacity retention has been measured after 75 cycles of charge–discharge. The current study demonstrated that the Sn–Co alloy with macroporous structure can be easily, conveniently and massively produced by a general template technique on relatively rough substrate (Ni-coated Cu sheet substrate). It is anticipated that the strategy of preparing macroporous Sn–Co alloy film can be also applied to synthesize other promising macroporous materials for lithium-ion batteries.

Acknowledgement

This work was supported by Major State Basic Research Development Program of China (2002CB2118004).

References

[1] J.O. Besenhard, J. Yang, M. Winter, J. Power Sources 68 (1997) 87.
[2] I.A. Courtney, J.R. Dahn, J. Electrochem. Soc. 144 (1997) 2045.
[3] I.A. Courtney, J.R. Dahn, J. Electrochem. Soc. 144 (1997) 2943.
[4] J. Xie, G.S. Cao, Y.D. Zhong, X.B. Zhao, J. Electroanal. Chem. 568 (2004) 323.
[5] H. Mukaibo, T. Sumi, T. Yokoshima, T. Momma, T. Osaka, Electrochem. Solid-State Lett. 6 (2003) A218.
[6] N. Tamura, R. Ohshita, M. Fujimoto, S. Fujitani, M. Kamino, I. Yonezu, J. Power Sources 107 (2002) 48.
[7] H. Li, G.Y. Zhu, X.J. Huang, L.Q. Chen, J. Mater. Chem. 10 (2000) 693.
[8] H. Li, X.J. Huang, L.Q. Chen, G.W. Zhou, Z. Zhang, D.P. Yu, Solid State Ionics 135 (2000) 181.
[9] L.H. Shi, H. Li, Z.X. Wang, X.J. Huang, L.Q. Chen, J. Mater. Chem. 11 (2001) 1502.
[10] N. Tamura, M. Fujimoto, M. Kamino, S. Fujitani, Electrochim. Acta 49 (2004) 1949.
[11] N. Tamura, Y. Kato, A. Mikami, M. Kamino, S. Fujitani, J. Electrochem. Soc. 153 (2006) A1626.
[12] J.J. Zhang, Y.Y. Xia, J. Electrochem. Soc. 153 (2006) A1466.
[13] C. Kim, M. Noh, M. Choi, J. Cho, B. Park, Chem. Mater. 17 (2005) 3297.
[14] J. Wolfenstine, S. Campos, D. Foster, J. Read, W.K. Behl, J. Power Sources 109 (2002) 230.
[15] J.C. Lytle, H. Yan, N.S. Ergang, W. Smyrl, A. Stein, J. Mater. Chem. 14 (2004) 1616.
[16] H. Yan, S. Sokolov, J.C. Lytle, A. Stein, F. Zhang, W.H. Smyrl, J. Electrochem. Soc. 150 (2003) A1102.
[17] H. Take, T. Matsumoto, K. Yoshino, Synth. Metals 135–136 (2003) 731.
[18] H. Take, H. Kajii, K. Yoshino, Synth. Metals 121 (2001) 1313.
[19] K.T. Lee, J.C. Lytle, N.S. Ergang, S.M. Oh, A. Stein, Adv. Funct. Mater. 15 (2005) 547.
[20] J. Fan, T. Wang, C.Z. Yu, B. Tu, Z.Y. Jiang, D. Zhao, Adv. Mater. 16 (2004) 1432.
[21] H.C. Shin, M.L. Liu, Adv. Funct. Mater. 15 (2005) 582.
[22] N.S. Ergang, J.C. Lytle, H. Yan, A. Stein, J. Electrochem. Soc. 152 (2005) A1989.
[23] F.S. Ke, L. Huang, H.H. Jiang, H.B. Wei, F.Z. Yang, S.G. Sun, Electrochem. Commun. 9 (2007) 228.
[24] G. Luo, Z.J. Liu, L. Li, S.H. Xie, J.L. Kong, D. Zhao, Adv. Mater. 13 (2001) 286.
[25] J.W. Goowin, J. Hearn, C.C. Ho, R.H. Ottewill, Colloid Polym. Sci. 252 (1974) 464.
[26] L.Y. Hao, Y. Zhou, W.Q. Jiang, Y.R. Zhu, F.Q. Li, Y. Hu, Z.Y. Chen, Chem. J. Chin. Univ. 22 (2001) 1945.
[27] P.N. Bartlett, M.A. Ghanem, I.S. EI Hallag, P. de Groot, A. Zhukov, J. Mater. Chem. 13 (2003) 2596.
[28] S. Rakers, L.F. Chi, H. Fuchs, Langmuir 13 (1997) 7121.
[29] L.H. Lu, R. Capek, A. Kornowski, N. Gaponik, A. Eychmiiller, Angew. Chem. 117 (2005) 6151.
[30] O.D. Velev, P.M. Tessier, A.M. Lenhoff, E.W. Kaler, Nature 401 (1999) 548.
[31] P.N. Bartlett, J.J. Baumberg, P.R. Birkin, M.A. Ghanem, M.C. Netti, Chem. Mater. 14 (2002) 2199.
[32] A. Lebugle, U. Axelsson, R. Nyholm, N. Martensson, Phys. Scr. 23 (1981) 825.
[33] C.D. Wagner, Disuss. Faraday Soc. 60 (1975) 291.
[34] J.F. Moulder, W.F. Stickle, P.E. Sobol, K.D. Bomben, Handbook of X-ray Photoelectron Spectroscopy, Physical Electronics, Inc., United States, 1995, p. 126.
[35] M. Winter, J.O. Besenhard, Electrochim. Acta 45 (1999) 31.
[36] M. Wachtler, M. Winter, J.O. Besenhard, J. Power Sources 105 (2002) 151.